Solar Energy 193 (2019) 502–506

Contents lists available at ScienceDirect

Solar Energy

journal homepage: www.elsevier.com/locate/solener

Optimization of SnO_2-based electron-selective contacts for Si/PEDOT:PSS heterojunction solar cells

Yupeng Zheng[a], Bing Jiang[a,*], Zhongliang Gao[a], Guilu Lin[b], Na Sang[b], Lei Chen[b], Meicheng Li[a]

[a] State Key Laboratory of Alternate Electrical Power System with Renewable Energy Sources, School of Renewable Energy, North China Electric Power University, Beijing 102206, China

[b] School of Mathematics and Physics, North China Electric Power University, Beijing 102206, China

ARTICLE INFO

Keywords:
Silicon heterojunction solar cells
Tin oxide
Electron-selective contact
Fermi level
Surface passivation

ABSTRACT

Tin oxide (SnO_2) is a potentially excellent electron-selective contact (ESC) for silicon (Si)-based solar cells due to its satisfactory energy band structure and good crystallinity. However, unsatisfactory electron extraction ability and limited surface passivating effect of SnO_2 ESCs will limit the performance of corresponding solar cells. We increase the Fermi level of SnO_2 by doping Ethylene diamine tetraacetic acid (EDTA), which endows EDTA-SnO_2 better electron extraction ability than SnO_2. Moreover, EDTA-SnO_2/SiO_x bilayer ESC prepared by combining a EDTA-SnO_2 layer and a thin silicon oxide (SiO_x) film provides better surface passivation than EDTA-SnO_2 ESC without impairing the charge transport capability markedly. The planar Si/PEDOT:PSS heterojunction solar cells (HSCs) with EDTA-SnO_2/SiO_x bilayer ESCs exhibit a power conversion efficiency (η) of 11.52%, which improves 13.7% in comparison with the η (10.13%) of HSCs with SnO_2 ESCs, mainly caused by the increase in V_{oc} and *FF* by 18 mV and 5.4% respectively.

1. Introduction

Due to its excellent device stability, high power conversion efficiency (η) and relatively mature industrial system, silicon (Si)-based solar cells occupy more than 90% of the photovoltaic market share. Further technical development direction of Si-based solar cells is to produce more efficient solar cells through simpler preparation process and lower cost. The working principle of the solar cell is that the light absorbing layer absorbs photons to generate electron and hole pairs, then the photogenerated electrons and holes transport under the driving force of Fermi level gradient (Wurfel et al., 2015). Carrier-selective contact (CSC), which extracts just one-type of carrier (electron or hole) from light absorbing layer, enables photogenerated electrons and holes transport to respective electrodes through different paths, thus realizing separation of carriers and utilization of photon energy (Bullock et al., 2018; Gao et al., 2018; Melskens et al., 2018; Yang et al., 2016). The most ideal solar cells should be constructed in the form of double heterojunction (Yablonovitch et al., 1985). In this structure, the narrow bandgap light absorbing layer is sandwiched between two oppositely doped wide bandgap layers that act as CSCs. Commercially available Si-based solar cells realize carrier separation by doping near-surface regions or preparing Si-based thin films to form CSCs (Bullock et al., 2018; Melskens et al., 2018; Yang et al., 2016). However, parasitic absorption, Auger recombination and other heavy doping effects caused by doped silicon contacts will limit the η of Si-based solar cells. Meanwhile, it requires high production cost and complicated process to prepare such contacts. Therefore, many researchers are devoted to developing better dopant-free CSCs (Bullock et al., 2018; Melskens et al., 2018; Yang et al., 2016).

When non-heavily doped silicon directly contacting silver (Ag) or aluminum electrodes in Si/PEDOT:PSS heterojunction solar cells (HSCs), high Schottky barrier caused by Fermi level pinning effect in the silicon surface area will hinder the carrier transmission, thus severely damaging the performance of solar cells (Bullock et al., 2018; He et al., 2018; Liu et al., 2017; Melskens et al., 2018; Wan et al., 2017; Yang et al., 2016; Yang et al., 2017; Yoon and Khang, 2018; Zhang et al., 2014). Therefore, preparing electron-selective contacts (ESCs) to promote the separation of photogenerated carriers, passivate the silicon surface and eliminate the Si/metal Schottky barrier are of great significance for improving the η of such HSCs. Metal oxide semiconductors such as titanium oxide (TiO_x) (Cui et al., 2016; Liao et al., 2014; Melskens et al., 2016; Yang et al., 2016), zinc oxide (ZnO) (Robertson, 2000), tin oxide (SnO_2) (Chen et al., 2018; Young et al., 2014) and tantalum oxide (TaO_x) (Wan, 2015) have been investigated as ESCs for Si-based solar cells due to their ease of deposition and low cost (Yang et al., 2016). Among them, n-type semiconductor SnO_2 has a slightly

* Corresponding author.
E-mail address: bingjiang@ncepu.edu.cn (B. Jiang).

https://doi.org/10.1016/j.solener.2019.09.077
Received 26 August 2019; Received in revised form 20 September 2019; Accepted 24 September 2019

higher conduction band and a very deep valence band comparing to silicon (Ke et al., 2015; Yang et al., 2018). The ideal band structure provides SnO_2 excellent electron transmission and hole blocking capabilities. Moreover, SnO_2 has higher electron mobility than TiO_x and better stability than ZnO (An et al., 2017; Ke et al., 2015). Recently, SnO_2 ESCs has been employed in Si/PEDOT:PSS HSCs and the efficiency is increased due to Fermi level depinning effect of SnO_2 (Chen et al., 2018). These outstanding properties of SnO_2 make it a potentially excellent ESC for Si-based solar cells. However, it is reported that deposited indium-doped SnO_2 (ITO) ESCs on a silicon wafer cannot provide low contact resistivity and good surface passivation without further processing (Young et al., 2014). Furthermore, unsatisfactory electron extraction ability of SnO_2 will limit the performance of corresponding solar cells (Yang et al., 2018).

In this work, we present EDTA-SnO_2/SiO_x bilayer ESCs with better properties comparing to SnO_2 ESCs for Si/PEDOT:PSS HSCs. We improve the Fermi level of SnO_2 by doping trace amount of Ethylene diamine tetraacetic acid (EDTA), which endows EDTA-SnO_2 with better electron extraction ability than SnO_2. Moreover, EDTA-SnO_2/SiO_x bilayer ESC is prepared by combining a EDTA-SnO_2 layer and a thin silicon oxide (SiO_x) film grown on silicon surface. EDTA-SnO_2/SiO_x bilayer ESC provides better surface passivation than EDTA-SnO_2 without impairing the charge transport capability markedly. The properties of SnO_2-based ESCs are evaluated by considering both the contact resistivity and the surface passivation quality on silicon surfaces. The planar Si/PEDOT:PSS HSCs featuring EDTA-SnO_2/SiO_x bilayer ESCs exhibit a higher η (11.52%) comparing to the η (10.13%) of HSCs with SnO_2 ESCs, mainly caused by the increase in V_{oc} and *FF* by 18 mV and 5.4% respectively.

2. Experiment section

2.1. Materials and devices fabrication

0.04 mg of EDTA (Sigma Aldrich) was dissolved in 1 ml of water, and 15 wt% SnO_2 solution (Alfa Aesar) was diluted to 2.5 wt%. Then the two solutions were mixed in equal volume to prepare EDTA-SnO_2 solution. The concentration of solution was adjusted by dilution or heating evaporation. PEDOT:PSS (Heraeus, PH1000) solution was doped with 7 wt% ethylene glycol (Innochem) and 0.1 wt% TX-100 (Alfa). The silicon wafer used is (1 0 0)-oriented n-type (1–3 Ω·cm, 270 μm, Tian Jin upward technology development co., ltd.).

The silicon wafer was ultrasonically cleaned with acetone, ethanol and deionized water for 10 min respectively, and then soaked in hydrofluoric acid solution (13.3 wt%) for 6 min to remove the SiO_x. After that, HSCs without SnO_2 ESCs was directly plated with Ag electrode at the rear side; for HSCs with SnO_2 or EDTA-SnO_2 ESCs, SnO_2 or EDTA-SnO_2 solution was spin-coated at 3500 rpm for 20 s at the rear side, then the solvent was removed by heating (60 ℃, 30 min), followed by plating Ag rear electrode; for HSCs with EDTA-SnO_2/SiO_x bilayer ESCs, SiO_x was prepared through ultraviolet (UV)/O_3 photo-oxidation treatment for 4 min by UV ozone cleaning system (Moldovan et al., 2015), and then EDTA-SnO_2 was spin-coated in the same way as mentioned above, followed by plating Ag rear electrode. Finally, PEDOT:PSS solution was spin-coated on the silicon wafer at 5000 rpm for 50 s and then annealed at 120 ℃ for 15 min, followed by plating front gate Ag electrode.

2.2. Device characterization

The light *J-V* curves of the solar cells were measured using a Keithley 2400 source under ambient conditions at room temperature. The light source was calibrated by a standard silicon solar cell to match AM 1.5 G. The contact resistivity of the rear structures were measured using a Keithley 2400 source. The external quantum efficiency (EQE) of HSC was tested by Zolix SCS100 full function solar cell quantum efficiency test system. XPS was performed by ESCALAB 250Xi, Thermofisher Scientific. Kelvin probe force microscopy (KPFM) was carried out on Aglient Keysight AFM-5500. The minority carrier lifetime was measured by MDPspot system from Freiberg Instruments.

3. Results and discussion

It is reported that EDTA can modify the properties of transition metal oxides by providing its lone-pair electrons to the vacant d-orbital of the transition metal atoms (Li et al., 2017). Moreover, doping of EDTA in SnO_2 can lead to similar result (Yang et al., 2018). We doped trace amount of EDTA in SnO_2 to modify the electron extraction ability of SnO_2. Then, we spin-coated SnO_2 and EDTA-SnO_2 on silicon wafer respectively to test the reaction between EDTA and SnO_2 by XPS test, the results were shown in Fig. 1. After doping of EDTA, the XPS spectra of EDTA-SnO_2 shows an additional little peak located at approximately 400 eV, ascribed to N in EDTA. Meanwhile, the Sn 3d peaks of EDTA-SnO_2 shift to higher binding energy position by approximately 0.13 eV comparing to the pristine SnO_2, indicating that EDTA is bound to the SnO_2 instead of simple mixing. The specific process of the reaction is shown in Fig. S1. The surface potentials of SnO_2 and EDTA-SnO_2 were tested by KPFM and the Fermi levels were calculated. The details of calculation are described in Note S1. As is shown in Fig. 2, the Fermi level of EDTA-SnO_2 is −4.10 eV, which is 0.08 eV higher than that of SnO_2. Fig. 3 presents the energy band structures of different HSCs (more details are shown in Note S2) (Amorim et al., 2012; Ke et al., 2015; Melskens et al., 2018). SnO_2 has an energy band structure matched well with silicon. The extremely deep valence band of SnO_2 can block the transmission of holes from silicon to Ag rear electrode effectively, thus helping to separate the photogenerated electrons and holes.

In order to evaluate the impedance to carrier transmission of Si/Ag,

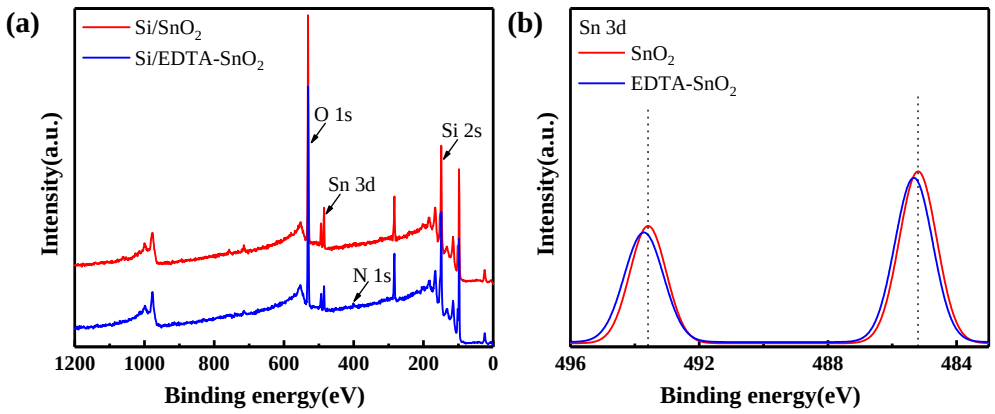

Fig. 1. (a) XPS spectra of SnO_2 and EDTA-SnO_2 on silicon. (b) XPS spectra of Sn 3d of SnO_2 and EDTA-SnO_2 on silicon.

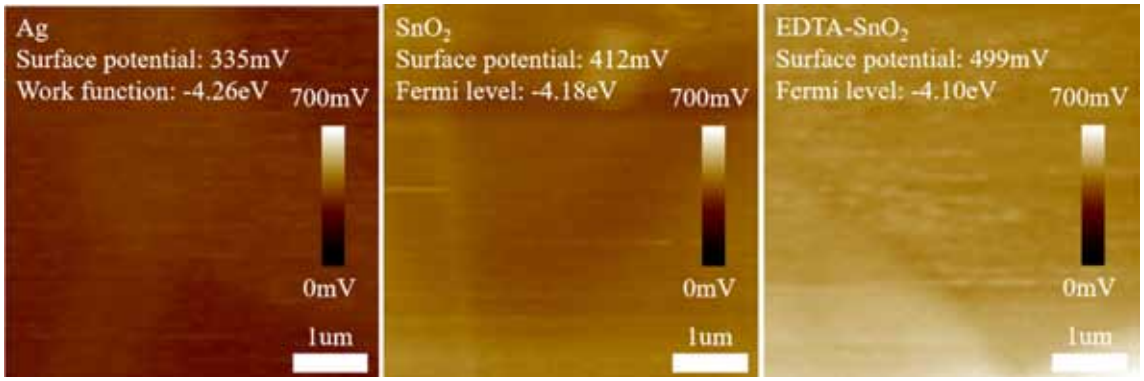

Fig. 2. Surface potentials and corresponding Fermi levels or work function of Ag, SnO_2 and EDTA-SnO_2 on silicon.

Si/SnO_2/Ag and Si/EDTA-SnO_2/Ag rear structures, we tested the resistance between two Ag rear electrodes of different structures. *J-V* curves of different rear structures and schematic diagram of the test structure are shown in Fig. 4. Due to the Fermi level pinning effect, high Schottky barrier (Φ_{B1} 0.56–0.76 eV) exhibits in Si/Ag contact (Huang and Hai, 1979). *J-V* curve of Si/Ag structure shows obvious rectification effect and high contact resistance. It is reported that there is a lower Schottky barrier (Φ_{B2} 0.31 eV) exhibits in SnO_2/metal contact (Amorim et al., 2012). Therefore, the lower resistance of Si/SnO_2/Ag structure than Si/Ag structure can be attributed to the lower barrier height caused the Fermi level depinning effect of SnO_2 on silicon surface. However, since SnO_2 prepared by spin coating is not uniformly coated on silicon surface (stronger Si 2s peak than Sn 3d peak found in Fig. 1(a)), Si/SnO_2/Ag structure still shows strong rectification effect. Moreover, Si/EDTA-SnO_2/Ag shows lowest contact resistance. According to the characteristics of n-type semiconductor/metal contacts, higher Fermi level of n-type semiconductor will be beneficial to reduce the width of the Schottky barrier caused by Fermi level pinning, thus facilitating the transmission of carriers. Therefore, EDTA-SnO_2 with higher Fermi level leads to lower contact resistivity comparing to SnO_2. The minority carrier lifetimes of Si, Si/SnO_2 and Si/EDTA-SnO_2 structures are all about 10 μs (more details are shown in Fig. S2), which means that carrier recombination rates on the silicon rear surfaces of all structures are very high. Therefore, although it is reported that SnO_2 will form Si-O-Sn bonds with silicon atoms (Chen et al., 2018), SnO_2 or EDTA-SnO_2 ESCs cannot passivate silicon surface effectively.

We prepared SnO_2 and EDTA-SnO_2 ESCs in Si/PEDOS:PSS HSCs and tested the corresponding photovoltaic performance. Fig. 5 shows the light *J-V* curves and EQE curves of the HSCs with different ESCs. Table 1 shows the photovoltaic parameters of different HSCs. HSCs without ESCs exhibits a moderate η of 9.31%, which is mainly limited by a relatively low V_{oc} (517 mV) and *FF* (64.5%). The V_{oc} of HSCs with SnO_2-based ESCs is markedly higher than that without ESCs, which is similar to the result that the V_{oc} was significantly increased after the insertion of TiO_x ESCs in p-n junction silicon solar cell (Yang et al., 2016). Higher V_{oc} means that photogenerated electrons and holes in the HSCs with ESCs can be better separated when voltage applied, which is just the original intention of inserting ESCs. The V_{oc} of HSCs with EDTA-SnO_2 ESCs is 5 mV higher than SnO_2 ESC, which is caused by the closer Fermi level of EDTA-SnO_2 to silicon conduction band. It is believed that higher Fermi level of ESC will be beneficial to extract electrons, thus enhancing the V_{oc} of solar cells (Snaith et al., 2010; Yang et al., 2018). In addition, due to the lower barrier width caused by higher Fermi level of EDTA-SnO_2, Si/EDTA-SnO_2/Ag exhibits lowest contact resistance. Therefore, due to better electron extraction ability and lower contact resistance, the *FF* of HSCs with EDTA-SnO_2 ESCs reaches 69.4% comparing to 65.8% of HSCs with SnO_2 ESCs. However, even though ESCs can help to separate photogenerated electrons and holes, the J_{sc} of the HSCs with SnO_2-based ESCs is just slightly higher than HSCs without ESCs. The EQE curves of HSCs with different rear structures are basically the same in the range of 550–1100 nm. The main reason is that SnO_2 and EDTA-SnO_2 cannot effectively passivate the dangling bonds on the silicon surface. Due to the lower barrier in the rear contact region caused by the insertion of ESCs in HSCs, the utilization of high-energy photons has been slightly improved.

As is known to all, a thin (about 1–2 nm) SiO_x film can chemically passivate the dangling bonds on the silicon surface and reduce the carrier recombination rate, which still allow carriers to transport between layers (Feldmann et al., 2014a, 2014b; Moldovan et al., 2015). Therefore, we place the silicon wafer under UV/O_3 photo-oxidation treatment for 4 min to produce a thin SiO_x passivation film with appropriate thickness, which is efficient and cheap (Moldovan et al., 2015). By preparing the SiO_x passivation film, the hydrophilicity of the silicon surface is significantly enhanced, which is beneficial to spin

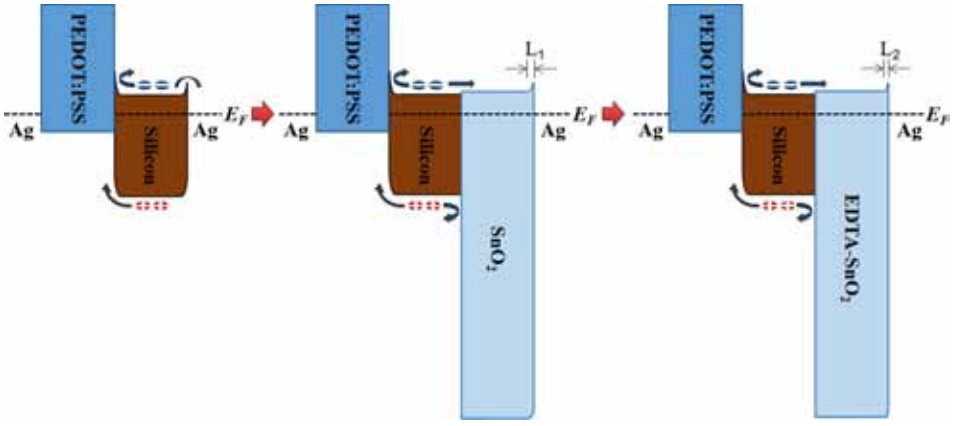

Fig. 3. Energy band structures of different Si/PEDOT:PSS HSCs.

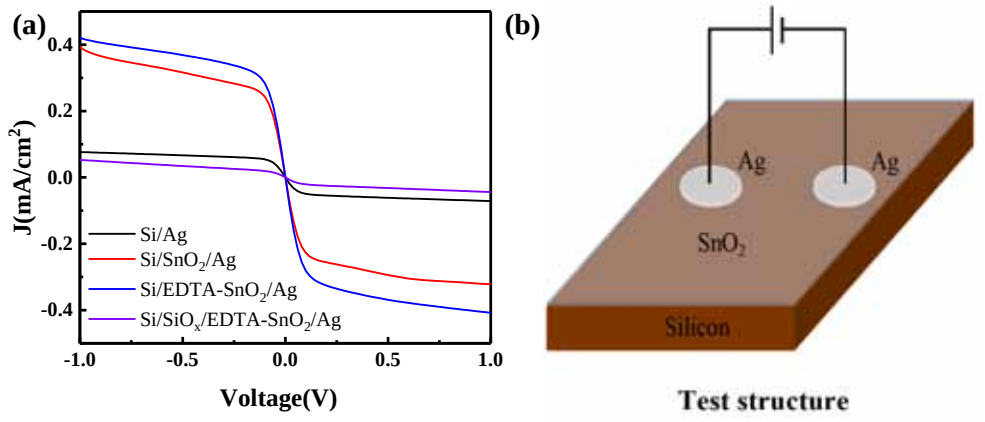

Fig. 4. (a) *J-V* curves of different rear structures. (b) Test structure of the resistance of different rear structures.

coating more uniform EDTA-SnO_2. We have prepared the Si/SiO_x/EDTA-SnO_2/Ag structure and evaluate the contact resistivity. The *J-V* of Si/SiO_x/EDTA-SnO_2/Ag structure is shown in Fig. 4. Through comparison, we find that the resistance of Si/SiO_x/EDTA-SnO_2/Ag is higher than Si/EDTA-SnO_2/Ag, which is caused by the high resistance of the SiO_x film. However, the rectification characteristic of the *J-V* curve of Si/SiO_x/EDTA-SnO_2/Ag is obviously weakened, mainly caused by more uniform EDTA-SnO_2 coating (more details are shown in Fig. S3). After oxidation passivation, the Si/SiO_x/EDTA-SnO_2 structure exhibits much higher minority carrier lifetime of 13.4 μs than other structures (about 10 μs), which indicates the lowest carrier recombination rate on the silicon surface. Fig. 5 presents the light *J-V* curve and EQE curve of HSCs with EDTA-SnO_2/SiO_x bilayer ESCs. Photovoltaic parameters of the HSCs are shown in Table 1. Due to more EDTA-SnO_2 coating and lower carrier recombination rate, HSCs with EDTA-SnO_2/SiO_x bilayer ESCs exhibit higher η than HSCs with EDTA-SnO_2 ESCs, which is mainly caused by the increase in V_{oc} and *FF* by 13 mV and 1.8% respectively. We note that increased contact resistance caused by a thin SiO_x film will not hinder the transmission markedly. Moreover, the EQE curve of the HSC with EDTA-SnO_2/SiO_x bilayer ESC is slightly improved in the range of 300–950 nm. The further increase of J_{sc} is ascribed to Fermi level depinning effect of EDTA-SnO_2 and reduction of carrier recombination rate on the silicon surface. After optimization, the planar Si/PEDOT:PSS HSCs with EDTA-SnO_2/SiO_x bilayer ESCs achieves a higher η of 11.52% than 10.13% of that with SnO_2 ESCs.

Table 1
Photovoltaic parameters of the HSCs with different rear structures.

Rear structure of HSC	V_{oc} (mV)	J_{sc} (mA/cm^2)	*FF* (%)	η (%)
Si/Ag	517 ± 5	28.0 ± 0.8	64.5 ± 3.0	9.31 ± 0.49
Si/SnO_2/Ag	544	28.3 ± 0.4	65.8 ± 0.7	10.13 ± 0.27
Si/EDTA-SnO_2/Ag	549 ± 4	28.2 ± 0.7	69.4 ± 2.0	10.75 ± 0.18
Si/SiO_x/EDTA-SnO_2/Ag	562 ± 5	28.8 ± 0.1	71.2 ± 0.2	11.52 ± 0.08

4. Conclusion

Due to its suitable energy band structure, SnO_2 ESC can help to separate photogenerated electrons and holes in Si/PEDOT:PSS HSC. Moreover, SnO_2 ESC can eliminate the high Schottky barrier caused by Si/Ag contact through Fermi level depinning effect. However, the performance of corresponding HSCs will be limited by the unsatisfactory electron extraction ability and limited surface passivation effect of SnO_2 ESCs. Through doping of EDTA, the Fermi level of EDTA-SnO_2 is closer to the conduction band of silicon than SnO_2, which will benefit the transmission of photogenerated electrons and enhance the V_{oc} of HSCs. Doping of EDTA also endues Si/EDTA-SnO_2/Ag lower contact resistivity than Si/SnO_2/Ag. Due to better separation of carriers and lower contact resistance, the *FF* of HSCs with EDTA-SnO_2 ESCs reaches 69.4% comparing to 65.8% of HSCs with SnO_2 ESCs. However, neither SnO_2 nor EDTA-SnO_2 can provide effective passivation for silicon surface. Therefore, EDTA-SnO_2/SiO_x bilayer ESC is prepared by combining a EDTA-SnO_2 layer and a thin SiO_x film grown on silicon surface. It is found that although SiO_x film increases the contact resistance of the rear region, the reduced carrier recombination rate and more uniform distributed EDTA-SnO_2 enables devices to have better performance. The planar Si/PEDOT:PSS HSCs with EDTA-SnO_2/SiO_x bilayer ESCs exhibit a higher η of 11.52% than 10.13% of that with SnO_2 ESCs, mainly caused by the improved V_{oc} and *FF*.

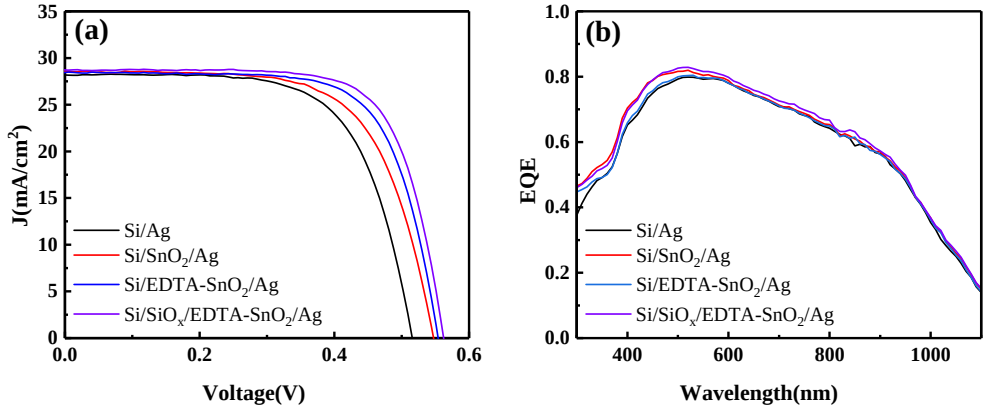

Fig. 5. (a) Light *J-V* curves of HSCs with different rear structures. (b) EQE curves of HSCs with different rear structures.

Acknowledgements

This work is supported partially by National Natural Science Foundation of China (No. 51772096), Beijing Municipal Science and Technology Project (Z181100005118002) and Science and Technology Beijing 100 Leading Talent Training Project.

Appendix A. Supplementary material

Supplementary data to this article can be found online at https://doi.org/10.1016/j.solener.2019.09.077.

References

Amorim, C.A., Berengue, O.M., Araújo, L., Leite, E.R., Chiquito, A.J., 2012. Gaussian distribution of Schottky barrier heights on SnO2 nanowires. In: Materials Research Society Symposium Proceedings. 1406, mrsf11-1406-z18-54.

An, Q., Fassl, P., Hofstetter, Y.J., Becker-Koch, D., Bausch, A., Hopkinson, P.E., Vaynzof, Y., 2017. High performance planar perovskite solar cells by ZnO electron transport layer engineering. Nano Energy S2211285517304238.

Bullock, J., Wan, Y., Xu, Z., Essig, S., Hettick, M., Wang, H., Ji, W., Boccard, M., Cuevas, A., Ballif, C., Javey, A., 2018. Stable dopant-free asymmetric heterocontact silicon solar cells with efficiencies above 20%. ACS Energy Lett. 3 (3).

Chen, L., Gao, Z., Zheng, Y., Cui, M., Yan, H., Wei, D., Dou, S., Ji, J., Jia, E., Sang, N., Liu, K., Ding, X., Li, Y., Li, M., 2018. 14.1% efficiency hybrid planar-Si/organic heterojunction solar cells with SnO_2 insertion layer. Sol. Energy 174, 549–555.

Cui, J., Allen, T., Wan, Y., Mckeon, J., Samundsett, C., Yan, D., Zhang, X., Cui, Y., Chen, Y., Verlinden, P., Cuevas, A., 2016. Titanium oxide: a re-emerging optical and passivating material for silicon solar cells. Sol. Energy Mat. Sol. C S0927024816301015.

Feldmann, F., Bivour, M., Reichel, C., Steinkemper, H., Hermle, M., Glunz, S.W., 2014a. Tunnel oxide passivated contacts as an alternative to partial rear contacts. Sol. Energy Mat. Sol. C 131, 46–50.

Feldmann, F., Simon, M., Bivour, M., Reichel, C., Hermle, M., Glunz, S.W., 2014b. Carrier-selective contacts for Si solar cells. Appl. Phys. Lett. 104 (18), 181105.

Gao, P., Yang, Z., He, J., Yu, J., Liu, P., Zhu, J., Ge, Z., Ye, J., 2018. Dopant-free and carrier-selective heterocontacts for silicon solar cells: recent advances and perspectives. Adv. Sci. 5 (3).

He, J., Wan, Y., Gao, P., Tang, J., Ye, J., 2018. Over 16.7% Efficiency organic-silicon heterojunction solar cells with solution-processed dopant-free contacts for both polarities. Adv. Funct. Mater. 28 (34), 1802192.

Huang, K., Hai, R., 1979. Elementary Semiconductor Physics. Science Press, China.

Ke, W., Fang, G., Liu, Q., Xiong, L., Qin, P., Tao, H., Wang, J., Lei, H., Li, B., Wan, J., Yang, G., Yan, Y., 2015. Low-temperature solution-processed tin oxide as an alternative electron transporting layer for efficient perovskite solar cells. J. Am. Chem. Soc. 137 (21), 6730–6733.

Liao, B., Hoex, B., Aberle, A.G., Chi, D., Bhatia, C.S., 2014. Excellent c-Si surface passivation by low-Temperature atomic layer deposited titanium oxide. Appl. Phys. Lett. 104 (25), 253903.

Liu, J., Ji, Y., Liu, Y., Xia, Z., Han, Y., Li, Y., Sun, B., 2017. Doping-free asymmetrical silicon heterocontact achieved by integrating conjugated molecules for high efficient solar cell. Adv. Energy Mater. 1700311.

Li, X., Liu, X., Zhang, W., Wang, H.Q., Fang, J., 2017. Fullerene-free organic solar cells with efficiency over 12% based on EDTA-ZnO hybrid cathode interlayer. Chem. 29 (10), 4176–4180.

Melskens, J., Van De Loo, B.W.H., Macco, B., Black, L.E., Smit, S., Kessels, W.M.M., 2018. Passivating contacts for crystalline silicon solar cells: from concepts and materials to prospects. IEEE J. Photovolt. 8 (2), 373–388.

Melskens, J., Van de Loo, B.W.H., Macco, B., Scheerder, R.W.H.S., Kessels, W.M.M., 2016. Feasibility study of titanium dioxide as passivating electron-selective contact for crystalline silicon solar cells. In: 6th SiliconPV Conf., Chambery, France.

Moldovan, A., Feldmann, F., Zimmer, M., Rentsch, J., Benick, J., Hermle, M., 2015. Tunnel oxide passivated carrier-selective contacts based on ultra-thin SiO_2 layers. Sol. Energy Mat. Sol. C 142 S0927024815003177.

Robertson, J., 2000. Band offsets of wide-band-gap oxides and implications for future electronic devices. J. Vac. Sci. Technol. B Microelectron. Nanom. Struct. 18 (3).

Snaith, H.J., Ducati, C., 2010. SnO_2-Based dye-sensitized hybrid solar cells exhibiting near unity absorbed photon-to-electron conversion efficiency. Nano Lett. 10 (4), 1259–1265.

Wan, Y., Bullock, J., Cuevas, A., 2015. Passivation of c-Si surfaces by ALD tantalum oxide capped with PECVD silicon nitride. Sol. Energy Mat. Sol. C S0927024815002433.

Wan, Y., Samundsett, C., Bullock, J., Hettick, M., Allen, T., Yan, D., Peng, J., Wu, Y., Cui, J., Javey, A., Cuevas, A., 2017. Conductive and stable magnesium oxide electron-selective contacts for efficient silicon solar cells. Adv. Energy Mater. 1601863.

Wurfel, U., Cuevas, A., Wurfel, P., 2015. Charge carrier separation in solar cells. IEEE J. Photovolt. 5 (1), 461–469.

Yablonovitch, E., Gmitter, T., Swanson, R.M., Kwark, Y.H., 1985. A 720 mV open circuit voltage SiO_x:c-Si:SiO_x double heterostructure solar cell. Appl. Phys. Lett. 47 (11), 1211.

Yang, D., Yang, R., Wang, K., Wu, C., Zhu, X., Feng, J., Ren, X., Fang, G., Priya, S., Liu, S. (Frank), 2018. High efficiency planar-type perovskite solar cells with negligible hysteresis using EDTA-complexed SnO2. Nat. Commun. 9 (1).

Yang, X., Bi, Q., Ali, H., Davis, K., Schoenfeld, W.V., Weber, K., 2016. High-performance TiO_2-based electron-selective contacts for crystalline silicon solar cells. Adv. Mater. 28 (28), 5891–5897.

Yang, Z., Gao, P., He, J., Chen, W., Yin, W.Y., Zeng, Y., Guo, W., Ye, J., Cui, Y., 2017. Tuning of the contact properties for high-efficiency Si/PEDOT:PSS heterojunction solar cells. ACS Energy Lett. 2 (3), 556–562.

Yoon, S.S., Khang, D.Y., 2018. High Efficiency (> 17%) Si-Organic Hybrid solar cells by simultaneous structural, electrical, and interfacial engineering via low-temperature processes. Adv. Energy Mater. 1702655.

Young, D.L., Nemeth, W., Grover, S., Norman, A., Yuan, H.C., Lee, B.G., Lasalvia, V., Stradins, P., 2014. Carrier selective, passivated contacts for high efficiency silicon solar cells based on transparent conducting oxides. Energy Procedia.

Zhang, Y., Liu, R., Lee, S.T., Sun, B., 2014. The role of a LiF layer on the performance of poly(3,4-ethylenedioxythiophene):poly(styrenesulfonate)/Si organic-inorganic hybrid solar cells. Appl. Phys. Lett. 104 (8), 083514.